AGU PUBLICATIONS

Geochemistry, Geophysics, Geosystems

RESEARCH ARTICLE
10.1002/2014GC005694

Special Section:
The Lithosphere-Asthenosphere System

An upper mantle seismic discontinuity beneath the Galápagos Archipelago and its implications for studies of the lithosphere-asthenosphere boundary

Joseph S. Byrnes[1], Emilie E. E. Hooft[1], Douglas R. Toomey[1], Darwin R. Villagómez[1,2], Dennis J. Geist[3], and Sean C. Solomon[4]

[1]Department of Geological Sciences, University of Oregon, Eugene, Oregon, USA, [2]Now at ID Analytics, San Diego, California, USA, [3]Department of Geological Sciences, University of Idaho, Moscow, Idaho, USA, [4]Lamont-Doherty Earth Observatory, Columbia University, Palisades, New York, USA

Key Points:
- A discontinuous decrease in wave speed with depth marks the base of dry mantle
- The base of dry mantle is deeper over the plume than under the spreading center
- Mantle upwelling and melting occur above the seismic discontinuity

Correspondence to:
J. S. Byrnes,
jbyrnes@uoregon.edu

Citation:
Byrnes, J. S., E. E. E. Hooft, D. R. Toomey, D. R. Villagómez, D. J. Geist, and S. C. Solomon (2015), An upper mantle seismic discontinuity beneath the Galápagos Archipelago and its implications for studies of the lithosphere-asthenosphere boundary, *Geochem. Geophys. Geosyst.*, *16*, 1070–1088, doi:10.1002/2014GC005694.

Received 17 DEC 2014
Accepted 25 FEB 2015
Accepted article online 2 MAR 2015
Published online 11 APR 2015

Abstract An upper mantle seismic discontinuity (the Gutenberg or G discontinuity), at which shear wave velocity decreases with depth, has been mapped from *S*-to-*p* conversions in radial receiver functions recorded across the Galápagos Archipelago. The mean depth of the discontinuity is 91 ± 8 km beneath the southeastern archipelago and 72 ± 5 km beneath surrounding regions. The discontinuity appears deeper beneath the portion of the Nazca plate that we infer passed over the Galápagos mantle plume than elsewhere in the region. We equate the depth of the G discontinuity to the maximum depth extent of anhydrous melting, which forms an overlying layer of dehydrated and depleted mantle. We attribute areas of shallow discontinuity depth to the formation of the dehydrated layer near the Galápagos Spreading Center and areas of greater discontinuity depth to its modification over a mantle plume with an excess temperature of 115 ± 30°C. The G discontinuity lies within a high-seismic-velocity anomaly that we conclude forms by partial dehydration and a gradual but steady increase in seismic velocity with decreasing depth after upwelling mantle first encounters the solidus for volatile-bearing mantle material. At the depth of the solidus for anhydrous mantle material, removal of remaining water creates a sharp decrease in velocity with depth; this discontinuity may also mark a site of melt accumulation. Results from seismic imaging, the compositions of Galápagos lavas, and rare-earth-element concentrations across the archipelago require that mantle upwelling and partial melting occur over a broad region within the dehydrated and depleted layer. We conclude that the G discontinuity beneath the archipelago does not mark the boundary between rigid lithosphere and convecting asthenosphere.

1. Introduction

Plate tectonics is broadly defined as the steady movement of colder, more rigid lithospheric plates over hotter, more ductile asthenosphere. The lithosphere and asthenosphere are further distinguished thermally by conductive versus advective heat transfer, respectively, because the lithosphere does not convect internally, whereas the asthenosphere does. Seismic studies have documented a seismic discontinuity in the upper mantle beneath ocean basins, historically known as the Gutenberg or G discontinuity [*Gutenberg*, 1948; *Gaherty et al*., 1996; *Bagley and Revenaugh*, 2008], which has often been interpreted as the "lithosphere-asthenosphere boundary" or LAB [*Fischer et al*., 2010; *Kind et al*., 2012]. This interpretation implies that the transition from lithosphere to asthenosphere, or from conductive to advective regimes, is sharp on the scale of a seismic wavelength [*Rychert et al*., 2005, 2007; *Kawakatsu et al*., 2009]. However, the physical processes that give rise to a seismically detectable interface are controversial [*Kawakatsu et al*., 2009; *Karato*, 2012; *Rychert et al*., 2012; *Schmerr*, 2012; *Karato*, 2014], as is the attribution of the G discontinuity to the LAB.

Under the simplest models, the formation of the oceanic lithosphere is by cooling [*Parsons and McKenzie*, 1978; *Faul and Jackson*, 2005], and a seismically sharp interface is not expected [*Stixrude and Lithgow-Bertelloni*, 2005]. By these models, the transition from lithosphere to asthenosphere occurs as minerals lose their strength at elevated temperatures and the lithosphere gradually thickens, approximately as the square root of the age of the plate. Because conductive cooling is gradual and continuous, the higher seismic velocities of the lithosphere should grade into the lower seismic velocities of the asthenosphere over a length scale

that is greater than the seismic wavelength typically used to map upper mantle discontinuities [*Stixrude and Lithgow-Bertelloni*, 2005].

Alternatively, models of oceanic lithosphere that include the effects of compositional layering and melt formation and transport can produce a seismically sharp interface in the upper mantle [*Karato and Jung*, 1998; *Karato*, 2012; *Olugboji et al*., 2013]. In particular, the water content of olivine markedly affects the viscosity [*Karato*, 1986; *Hirth and Kohlstedt*, 1996; *Phipps Morgan*, 1997] and seismic velocity [*Karato and Jung*, 1998; *Aizawa et al*., 2008] of the upper mantle, with anhydrous olivine predicted to be more viscous (by orders of magnitude), and higher in seismic velocity, than partially hydrated olivine. Because water preferentially partitions into melt, the residuum of mantle melting is predicted to be stronger and higher in seismic velocity than unmelted mantle material. Under this scenario, the rheology of oceanic mantle reflects its melting history. Thus, the depth at which relatively strong, high-velocity mantle is predicted to occur depends only on the depth at which anhydrous melting starts within upwelling mantle and is more or less independent of lithospheric age [*Hirth and Kohlstedt*, 1996; *Phipps Morgan*, 1997].

Oceanic hotspots are an ideal setting to test if upper mantle seismic discontinuities are thermally or compositionally controlled and whether seismic discontinuities are associated with a LAB. This opportunity arises because the temperatures and compositions of hotspots affect both the thermal structure of the surrounding mantle and the depth of mantle melting. The addition of heat by hotspot upwelling causes mantle isotherms to shoal [*Detrick and Crough*, 1978], resulting in thinning of the thermal lithosphere [*Li et al*., 2004; *Mittelstaedt et al*., 2011]. Elevated temperatures, however, also drive melting and dehydration of the mantle to greater depths, which produces a thicker layer of relatively high viscosity and high seismic velocity [*Phipps Morgan et al*., 1995; *Hall and Kincaid*, 2003]. Larger volatile contents in a mantle plume may further deepen the initiation of melting [*Asimow and Langmuir*, 2003; *Asimow et al*., 2004]. Thermal and compositional models of the oceanic upper mantle therefore predict opposite changes in the rheologic and seismic structure of the upper mantle when overriding a hotspot.

Results of previous studies are equivocal on the thermal or compositional origin of upper mantle seismic discontinuities beneath oceanic plates. The Gutenberg (G) discontinuity [*Gutenberg*, 1948], at which velocity decreases sharply with depth, is typically located between 40 and 100 km depth. Many workers have interpreted this discontinuity as the base of the lithosphere [e.g., *Rychert and Shearer*, 2009; *Rychert et al*., 2010; *Kind et al*., 2012, *Schmerr*, 2012]. Moreover, many studies of this seismic discontinuity beneath the Pacific plate indicate that it deepens with age, as expected for a plate that thickens by conductive cooling [*Kawakatsu et al*., 2009; *Kumar and Kawakatsu*, 2011; *Rychert and Shearer*, 2011; *Schmerr*, 2012], though for young ($<$30 Ma) lithosphere the depth of the discontinuity identified from SS precursors is greater (50–55 km) than expected [*Schmerr*, 2012]. The seismic discontinuity beneath Hawai'i is observed to shoal along the hotspot chain, which is consistent with a feature that is thermally controlled [*Li et al*., 2004]. Another hypothesis, which is related to a thermal origin for the G discontinuity, is that accumulation of melt at the base of the thermal lithosphere creates the observed sharp discontinuity in seismic velocity [*Kawakatsu et al*., 2009; *Hirschmann*, 2010; *Schmerr*, 2012].

On the other hand, the depth of the upper mantle discontinuity beneath most hotspots and some oceanic plates is consistent with the base of a high-viscosity, dehydrated mantle layer. Analysis of receiver functions from the Cape Verde Islands and Hawai'i indicated the presence of a dehydrated and depleted root [*Lodge and Helffrich*, 2006; *Rychert et al*., 2013]. Similarly, upper mantle seismic discontinuities beneath Amsterdam Island, Easter Island, the Galápagos Archipelago, and Iceland are all deeper (50–80 km) than the predicted depth of the thermal boundary layer at the corresponding crustal ages [*Vinnik et al*., 2005; *Kumar et al*., 2005; *Heit et al*., 2007; *Kumar et al*., 2007; *Rychert et al*., 2014]. Several workers have also observed a G discontinuity beneath the Pacific and Philippine plates at depths that are inconsistent with the base of conductively cooled lithosphere [*Gaherty et al*., 1996, 1999; *Bagley and Revenaugh*, 2008; *Tonegawa and Helffrich*, 2012]. *Beghein et al*. [2014] found that the depth of the G discontinuity beneath the Pacific is independent of plate age and inferred that it is likely formed by dehydration of the topmost mantle at the spreading center and the presence of seismic anisotropy due to lattice preferred orientation below the dehydrated layer.

In this paper, we investigate the structure of the upper mantle seismic G discontinuity beneath the Galápagos Archipelago using *S*-to-*p* conversions identified in radial receiver functions derived from teleseismic body waves that were recorded by a temporary broadband array. We aim to test whether

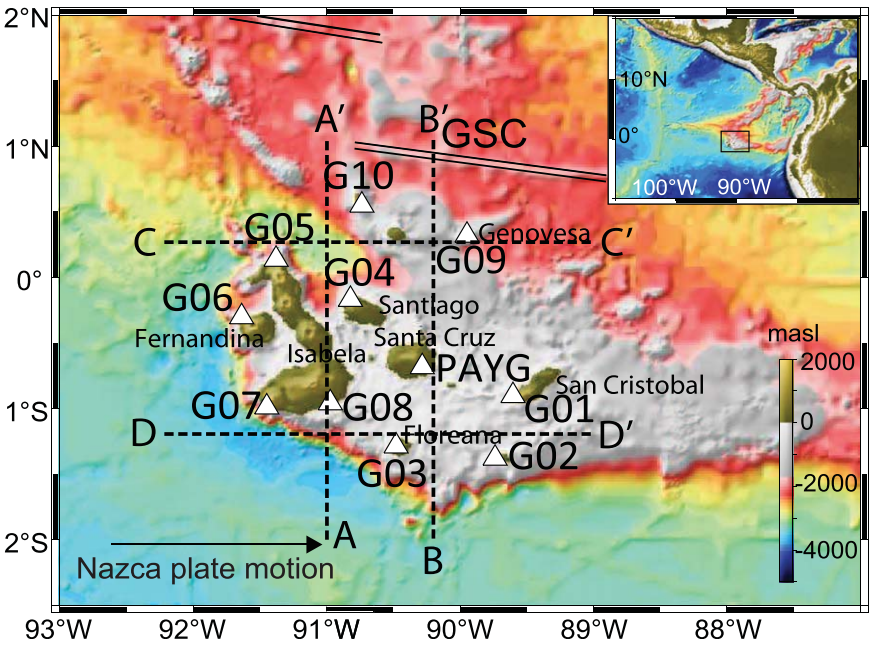

Figure 1. Map of the Galápagos Archipelago and the seismic network. White triangles are seismic stations. Stations with names that begin with G formed the temporary array; PAYG is part of the GSN. The Galápagos Spreading Center (GSC) and the direction of Nazca plate motion in a hotspot reference frame [*Gripp and Gordon*, 2002] are shown. The dashed lines show the locations of the profiles in Figures 2 and 5. Inset shows the broader setting of the study area.

thermal or compositional processes define the G discontinuity, and if the G discontinuity separates the lithosphere from the asthenosphere. The Galápagos Archipelago is an ideal setting because the young seafloor age [*Hey and Vogt*, 1977; *Barckhausen et al*., 2001] predicts a thin thermal lithosphere. In addition, previous studies provide detailed seismic images of the mantle velocity structure [*Villagómez et al*., 2007, 2014] and extensive information on the geochemistry of the lavas throughout the archipelago [*White et al*., 1993; *Graham et al.,* 1993; *Kurz and Geist*, 1999; *Harpp and White*, 2001; *Herzberg and Gazel*, 2009; *Gibson and Geist*, 2010]. *Rychert et al*. [2014] found a G discontinuity at 75 ± 12 km depth beneath the southwestern Galápagos, which they interpreted to be caused by depletion and dehydration in the upper mantle. We find a similarly deep G discontinuity, but the area can be separated into distinct regions of differing discontinuity depth. We show that mantle melting, volatile removal, and their physical effects can explain the change in discontinuity depth and the associated mantle velocity structure. Moreover, by comparing the structure of this interface with the mantle seismic velocities and the inferred mantle melting depths, we conclude that above the G discontinuity the mantle is flowing upward and melting over a broad region. Thus, the seismic interface does not represent the base of the rigid lithosphere or coincide with the LAB. Our results may have implications for the interpretation of upper mantle discontinuities beneath oceanic plates in other locations.

2. Seismic Data and Receiver Functions

We analyzed seismic data from 10 portable, three-component broadband stations that were installed across the Galápagos Archipelago from September 1999 to April 2002 (Figure 1). The instrumentation used was described by *Hooft et al*. [2003]. The array was augmented by the permanent Global Seismographic Network (GSN) station PAYG on the island of Santa Cruz. The aperture of the seismic array was 300 km by 200 km, and the station spacing was 50–70 km.

We used the radial receiver function method to identify seismic discontinuities from *S*-to-*p* conversions in the upper mantle beneath the network. Energy converted from *S* to *P* waves arrives before the primary *S* phase and so is not contaminated by crustal reverberations (particularly the reflections from the crust-mantle boundary), making *S*-to-*p* conversions ideal for studies of the upper mantle. Since the converted *p* wave refracts at a larger angle of incidence than that of the direct *S* wave, the footprint of *S*-to-*p*

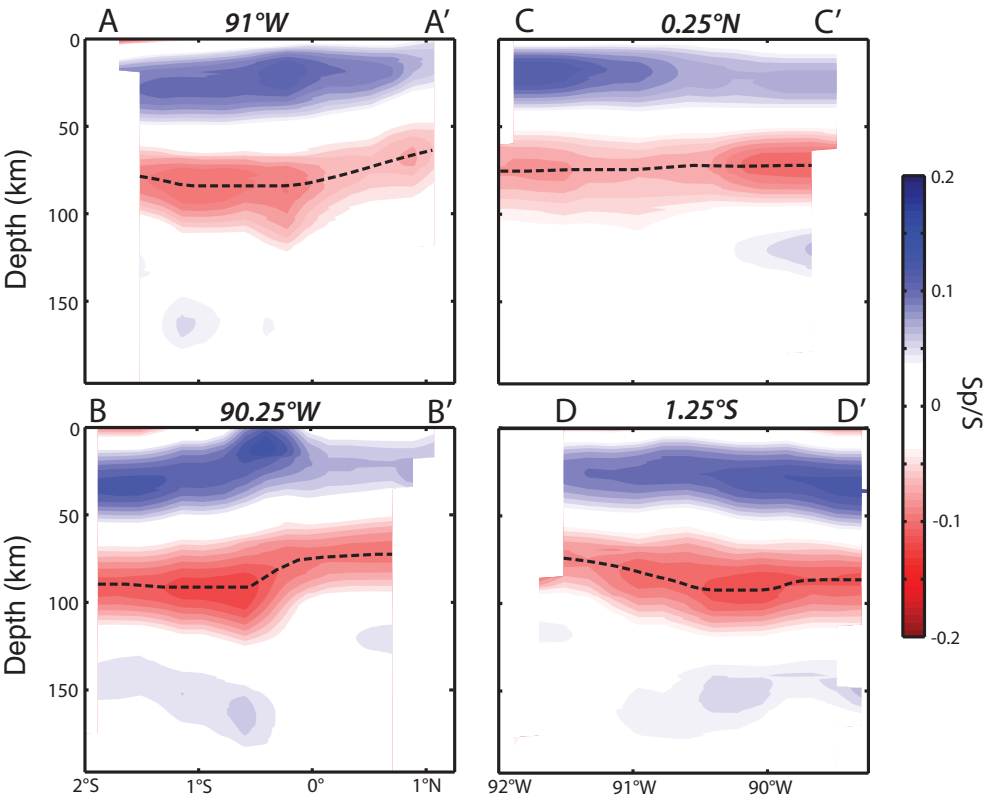

Figure 2. Depth sections through the CCP stack of the *S*-to-*p* receiver functions. (a, b) Cross sections in the south-to-north direction. (c, d) Cross sections in the west-to-east direction. The locations of the cross-sections are shown in Figure 1. The dashed line in each plot marks the depth of the largest negative amplitude of the CCP stack. The amplitude (*Sp*/*S*) of the CCP stack is the ratio of the amplitude of the *S*-to-*p* converted phase to that of the direct *S* arrival.

conversions is also larger than that for *P*-to-*s* conversions. On the other hand, conversions from *S* phases are noisier and the usable signal is lower in frequency than for *P* phases. In this study, we used the *S* or *SKS* phase from 29 teleseismic events located at 60°–115° epicentral distance. Events were visually selected, records were rotated into the *P-SV-SH* coordinate system [*Vinnik*, 1977], and the rotated traces were bandpass filtered between 0.01 and 2 Hz before processing.

Receiver functions were calculated using the extended-time, multitaper deconvolution method [*Park et al*., 1987; *Park and Levin*, 2000; *Helffrich*, 2006]. To smooth the source spectra, the traces were divided into 10-s-long segments with 50% overlap. Spectra for each segment were calculated with three Slepian tapers and a half-bandwidth parameter of 2.5, and then all the spectra were averaged [*Helffrich*, 2006]. After spectral division, the receiver functions were bandpass filtered between 0.03 and 0.1 Hz to avoid the microseismic noise peak [*Webb*, 1998]. On the basis of visual inspection, traces that had a poor signal-to-noise ratio or that appeared monochromatic were removed from our analysis. To plot the arrival times and polarities of the receiver functions as are done for the more common *P*-to-*s* receiver functions, the time axis and polarity were reversed.

The results of 96 receiver functions are presented using three separate stacking procedures. First, a common conversion point (CCP) stack was calculated [*Dueker and Sheehan*, 1998; *Hansen and Dueker*, 2009] by migrating the receiver functions to depth through the velocity model of *Villagómez et al*. [2014] (Figure 2). The CCP stack was binned at 20 km intervals and was averaged horizontally over 140 km and was not averaged vertically. Bins with less than five receiver functions after horizontal averaging were rejected. A map of the migrated depth of the negative phase (Figure 3a, dashed lines in Figures 2 and 5) was made by taking the minimum value of the CCP stack above 150 km depth.

Second, inspection of the CCP stack revealed two regions of differing discontinuity depth, motivating us to stack separately the receiver functions in these two regions. A stack of receiver functions from the

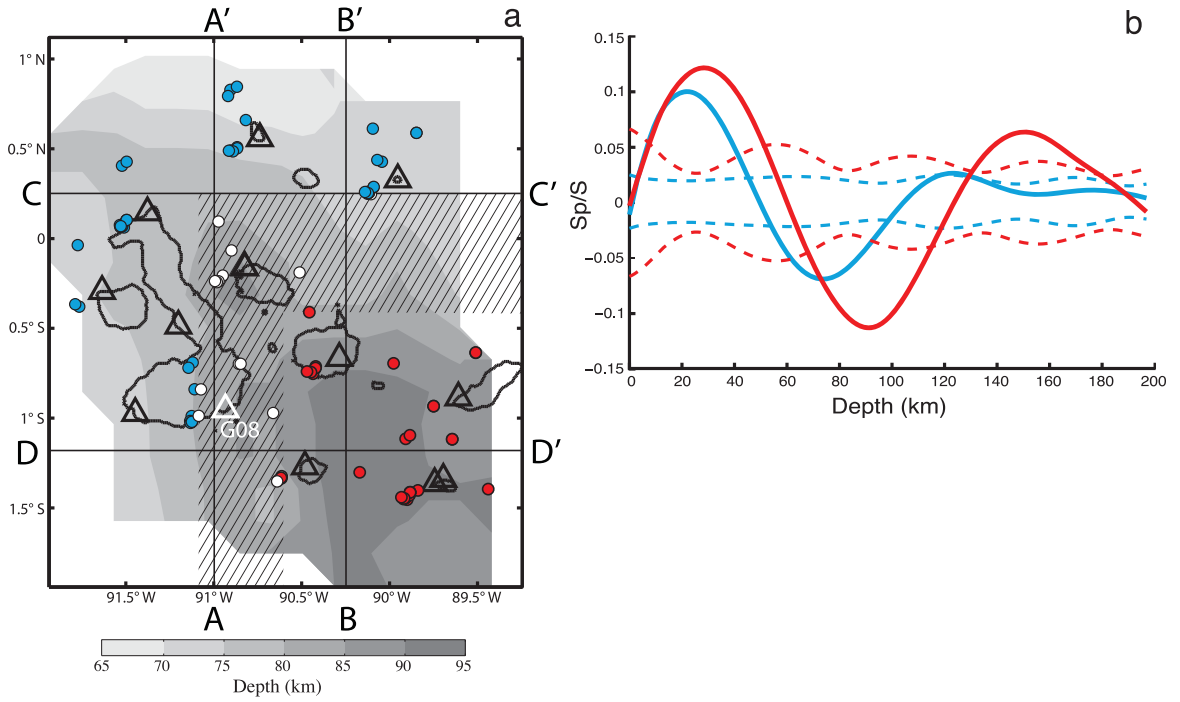

Figure 3. Depth to the conversion point of the negative receiver function phase beneath the Galápagos Archipelago and receiver function stacks within the southeastern archipelago and surrounding region. (a) Contour map of the depth (gray scale) to the negative phase in the CCP stack of the receiver functions. The stations are shown as triangles, with station G08 labeled in white (see text for discussion). The islands are outlined. The solid lines show the locations of the profiles in Figures 2 and 5. The piercing points of the receiver functions at 80 km depth are shown as 30 red and 50 blue circles for conversion points deeper and shallower than this depth, respectively; the 16 white circles could be included in either region. The hachured area reflects the uncertainty in the boundary between the southeastern archipelago and the surrounding region. See text for discussion. (b) Stacks of the receiver functions from the southeastern archipelago (red solid line) and surrounding region (blue solid line) plotted as functions of depth. The dashed lines show twice the standard error of the mean for each stack in the corresponding color. The amplitude of the stacks is scaled as in Figure 2.

southeastern quadrant of the archipelago was compared with a stack from the rest of the study area (Figures 3 and 4b and d). The latitudinal and longitudinal boundaries of the southeastern quadrant were estimated by a grid search that sought to maximize the difference in the depth of the G discontinuity between that quadrant and the surrounding region. During the grid search, only boundaries of the southeastern quadrant that included 20 or more receiver functions in both the southeastern archipelago and surrounding region were considered. Standard errors for the amplitude of the phases in these two stacks were found by calculating the standard error of the mean for the stack of receiver functions (shown by the dashed lines in Figures 3b, 4b, d, and f), and the errors in the inferred depth of the phases were found by bootstrapping with 1000 samples; all reported uncertainties are twice the standard error, σ.

Third, to probe upper mantle structure directly over the location of the inferred Galápagos plume at 150 to 200 km depth [*Villagómez et al*., 2014], we separately stacked receiver functions in the southwestern archipelago (specifically within 50 km of station G08, Figures 4e and 4f). Errors for the amplitude and depth of phases in this stack were found by the same method as for the two regional stacks. We note that our data set does not provide spatial coverage to determine the G discontinuity structure immediately west of the plume location (Figure 3a).

3. Results

In the Galápagos Archipelago, we identify two clear *S*-to-*p* converted phases in the CCP stack, a positive phase at ~20 km depth and a negative phase at ~80 km depth (Figure 2). We associate the positive-polarity phase with the velocity increase (with increasing depth) at the crust-mantle boundary or Moho. We identify the negative phase with the G discontinuity, a common label for the base of the high seismic velocity layer in the oceanic upper mantle [e.g., *Gaherty et al*., 1996, 1999; *Bagley and Revenaugh*, 2008]. A third, low-amplitude, positive-polarity phase may be indicated in records from the southeastern archipelago at

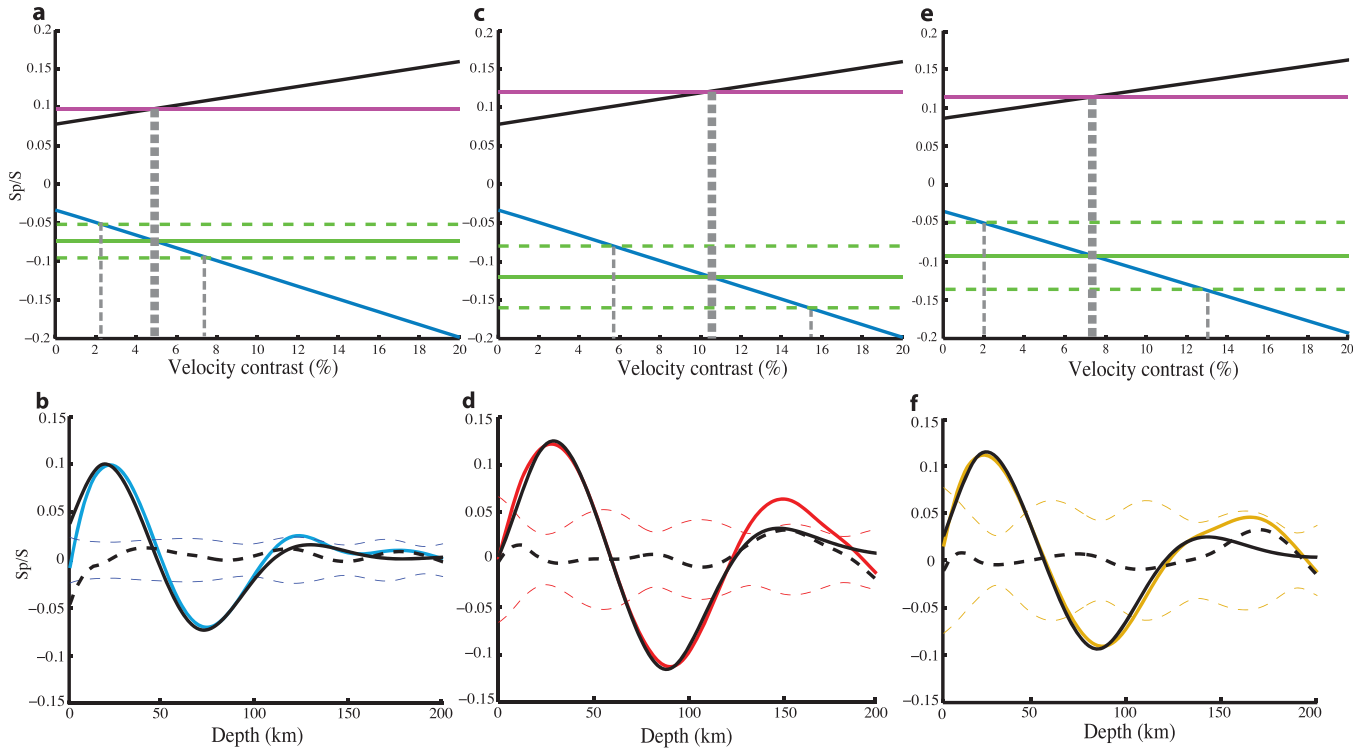

Figure 4. Waveform modeling of the three receiver function stacks from the surrounding portions of the archipelago (left column), the southeastern archipelago (middle column), and the region over the Galápagos mantle plume (right column). (Top row: a, c, and e) Amplitudes of the positive (black lines) and negative (blue lines) phases in synthetic receiver functions as functions of the velocity contrast across the G discontinuity; see text for details. The observed amplitude of the positive phase (conversion at the Moho, magenta line) and the negative phase (conversion at the G discontinuity, green line) for each receiver function stack are shown (dashed green lines show the uncertainty in the amplitude of the negative phase). The best-fitting velocity contrast is chosen by matching the observed and modeled negative-phase amplitudes (bold gray dashed line), and the error in the velocity contrast (thin gray dashed lines) corresponds to the uncertainty in the amplitude of the negative phase. (Bottom row: b, d, and f) Comparison of the receiver function stack from the surrounding portions of the archipelago, the southeastern archipelago, and the region over the Galápagos mantle plume (blue, red, and yellow, respectively) with the best-fitting synthetic receiver function for each region (black). The residual receiver function (black dashed line) is the difference between the observed and synthetic receiver function and represents structure in the receiver function that we have not modeled. The significance of the residual receiver function can be inferred relative to two standard errors for the stack (dashed lines in the color corresponding to each region).

~150 km depth. In this paper, we focus on the negative-polarity G phase at ~80 km depth, because the long wavelength of *S*-to-*p* phases relative to the depth to the base of the crust limits the resolution of the shallowest discontinuity, and the phase from ~150 km depth is small in amplitude and waveform modeling suggests that it may be an artifact, as discussed below.

A map of the depth of the phase conversion associated with the negative phase (Figure 3) reveals that the G discontinuity in the southeastern quadrant of the study area is systematically deeper than in the rest of the archipelago. To quantify the difference in the discontinuity depth between these two regions, we used the grid search method, described above as the second stacking method, to stack the receiver functions (Figure 3). From that search, the resulting discontinuity depths are 91 ± 8 km in the southeastern archipelago and 72 ± 5 km in the surrounding region; i.e., the G discontinuity is 19 ± 9 km deeper in the southeastern portion of the area than elsewhere. The receiver function stacks for the two distinct regions do not change significantly if the borders of the southeastern quadrant are moved by approximately 0.5° in either the latitudinal or longitudinal direction (hachured region in Figure 3a).

The data in the areas where the G discontinuity transitions from relatively deep to shallow depths do not clearly resolve whether the change in the depth of the G discontinuity occurs as a step or a gradient. The western transition, near 91°W, is located above the location of the inferred Galápagos plume at 150–200 km depth (Figure 3c of *Villagómez et al.* [2014]). A stack of receiver functions with piercing points at 80 km depth that are within 50 km of site G08 shows a negative phase that migrates to a depth of 82 ± 10 km (Figure 4f). This G discontinuity depth is intermediate between that for the two regional stacks,

but within twice the standard error of each. The 82 ± 10 km depth could represent either an actual intermediate depth or a poorly resolved rapid transition from 72 to 91 km depth. Henceforth, we consider simply the two-region division between the "southeastern quadrant" and "surrounding regions" as shown in Figure 3a, unless otherwise noted.

The amplitude of the receiver functions can be used to constrain the velocity contrast across the G discontinuity. In the southeastern quadrant and the surrounding region, the amplitude of the G-discontinuity conversion normalized by the amplitude of the direct arrival is −0.12 ± 0.04 and −0.07 ± 0.02, respectively (Figures 3b and 4a and 4c). To estimate the associated velocity contrast, the amplitude of each observed stack was compared with a stack of synthetic receiver functions. The latter were generated for a range of *S*-wave velocity contrasts at the G discontinuity and two- and three-layer velocity models, using the same ray parameters as the observations. Two-layer models included a topmost mantle layer (4.5 km/s) and an underlying half-space, for which the velocity was varied but was less than the layer above. The three-layer models included an additional crustal layer (4 km/s), for which the velocity is consistent with the results of *Villagómez et al*. [2011]. The thickness of the crust (28 ± 9 km and 20 ± 4) and the depth to the G discontinuity (91 and 72 km) were taken from the results for the southeastern archipelago and surrounding region, respectively. Green's functions were calculated with a reflectivity algorithm [*Park*, 1996; *Levin and Park*, 1998], convolved with a synthetic source, and subsequently deconvolved and filtered following the same method as that used for the observed data. Densities were determined from the Nafe-Drake relation [*Brocher*, 2005]. We adopted a ratio of *P*-wave velocity to *S*-wave velocity, V_P/V_S, of 1.76, and attenuation was not included.

Our estimate of the shear velocity contrast at the G discontinuity depends on whether the Moho is or is not modeled simultaneously with the G discontinuity (three- and two-layer model, respectively). This dependence arises because the phases from the Moho and G discontinuity interfere, which affects their amplitudes. Figure 4 shows the results of synthetic modeling for three-layer models; two-layer models were treated in a similar manner. To estimate the velocity contrast at the G discontinuity, we varied the velocity of the half-space, measured the amplitude of the resulting Moho and G-discontinuity conversions on the synthetic receiver functions, and compared these directly with the observed amplitudes. The uncertainty in the amplitude of the observed G-discontinuity conversion was used to estimate the error in the velocity contrast at the G discontinuity (Figure 4). When we use the two-layer models (i.e., no Moho), we obtain shear velocity contrasts of 18 ± 5% and 11 ± 3% in the southeastern and surrounding regions, respectively. By including a Moho interface and matching the amplitude of both the positive and negative phases, we infer shear velocity contrasts of 11 ± 5% and 5 ± 3% in the southeastern archipelago and surrounding region, respectively. Our estimate of the shear velocity contrast at the G discontinuity thus decreases by 6–7% in a three-layer versus a two-layer model. More complicated models are not required because of the long-period character and overall structure of the receiver functions. Additional modeling indicates that varying the velocity contrast at the Moho has a small effect on our estimate of the velocity contrast at the G discontinuity. Furthermore, our estimate of the arrival time of the conversion from the G discontinuity is insignificantly affected by interference with the Moho arrival. To evaluate this potential source of error, we compared the arrival time of the converted phase from the G discontinuity in impulsive Green's functions to the arrival time in synthetic receiver functions for a range of ray parameters. The difference in arrival time is equivalent to a change in the depth of the G discontinuity by ±1 km, which is well within our observational error.

The amplitude of a converted phase is also influenced by the sharpness of the associated discontinuity. Receiver functions are most sensitive to velocity gradients distributed over a depth range of less than half the wavelength of the incident phase [*Rychert et al*., 2007]. The dominant wavelength of the incident phase in our study is ~50 km. As a result, the velocity gradient could be distributed over a depth interval of 0 to ~25 km. Lower gradients produce smaller-amplitude converted phases. Since we estimated the shear velocity contrasts associated with our receiver function with abrupt discontinuities, our estimates of 11 ± 5% and 5 ± 3% are lower bounds.

The deeper positive-polarity phase observed in the southeastern archipelago at a depth of 150 km has an amplitude of 0.06 ± 0.04. A similar phase does not appear in the receiver function stack from the surrounding portion of the archipelago, and the phase is not resolved in a stack of receiver functions with piercing points beneath southern Isabela. Synthetic receiver functions show that the amplitude of this later positive-polarity phase is partially an artifact of deconvolution; the synthetic receiver functions that reproduce the

Moho and G-discontinuity conversions form a side lobe that has an amplitude approximately one quarter that of the adjacent negative phase (Figure 4). When corrected for this effect the amplitude of a possible phase converted near 150 km depth is less than twice the standard error (Figure 4); hence this phase does not indicate a discontinuity at high confidence.

The results presented here are consistent with previous receiver function studies in the Galápagos [*Heit et al*., 2007; *Rychert et al*., 2014]. *Heit et al*. [2007] calculated receiver functions from the GSN station PAYG, and *Rychert et al*. [2014] examined receiver functions from PAYG and an array (SIGNET) concentrated on the southern half of Isla Isabela. Our study has the advantage of both broader station coverage and inclusion of the regional mantle velocity model of *Villagómez et al*. [2014]. The use of this velocity model aids in the migration of the receiver functions to depth and, more importantly, provides a context for interpretation of the results. On the basis of stacks of receiver functions from all azimuths at PAYG, previous studies indicated a negative-polarity phase converted at a depth of 70 km [*Heit et al*., 2007] and 75 $\pm$ 12 km [*Rychert et al*., 2014], values consistent with our result for most of the Galápagos, 72 $\pm$ 5 km. With the SIGNET array, *Rychert et al*. [2014] mapped lateral variations in the depth of this phase from 66 to 82 km. That study had the best coverage in the southwestern archipelago, where *Rychert et al*. [2014] found the negative phase to originate from a depth between 76 and 80 km, a value within the error of that obtained in this study beneath southern Isabela, 82 $\pm$ 10 km. The broader spatial coverage of our study allows us to identify the greatest depth of the discontinuity, 91 $\pm$ 8 km, beneath the southeastern Galápagos. Given the poor resolution of the Moho, our results (28 $\pm$ 9 and 20 $\pm$ 4 km from the southeastern quadrant and surrounding regions, respectively) are broadly consistent with those of previous receiver function studies (30 and 37 $\pm$ 7 km, *Heit et al*. [2007] and *Rychert et al*. [2014], respectively).

Our estimates of the shear velocity contrast at the G discontinuity are similar to those found in other studies both near and away from oceanic hotspots. Beneath the Pacific plate, reported velocity contrasts are consistently 6–7% [*Gaherty et al*., 1996; *Tan and Helmberger*, 2007; *Kawakatsu et al*., 2009; *Schmerr*, 2012]. Beneath hotspots, reported shear velocity contrasts are somewhat larger and range from 8 to 20% [*Collins et al*., 2002; *Lodge and Helffrich*, 2006; *Wölbern et al*., 2006]. In the southeastern Galápagos, the velocity contrast, 11 $\pm$ 5%, is comparable with that at other oceanic hotspots, whereas elsewhere in the Galápagos the velocity contrast, 5 $\pm$ 3%, is similar to that beneath normal seafloor.

4. Discussion

We discuss our results in the context of previous studies of the Galápagos Archipelago and argue that: (1) the observed G discontinuity marks the base of fully dehydrated mantle (i.e., where dry silicate melting begins in upwelling mantle); (2) variations in the depth of the G discontinuity are consistent with estimates of the excess temperature of the Galápagos plume relative to the nearby spreading center; (3) mantle melting, volatile removal, and the physical effects of these processes can account for the depth of the G discontinuity, as well as tomographically imaged high-velocity anomalies, (4) the velocity contrast across the seismic discontinuity places bounds on likely variations in composition, water content, and partial melt; and (5) mantle upwelling and decompression melting occur above the G discontinuity, implying that the discontinuity is not the LAB. Each of these topics is addressed below.

4.1. Spatial Relationship of Seismic Velocity Anomalies and the G Discontinuity

Previous seismic imaging is consistent with an upwelling mantle plume beneath the Galápagos that shoals toward the Galápagos Spreading Center and is overlain by a high-velocity anomaly formed by chemical depletion and dehydration [*Villagómez et al*., 2007, 2014]. Moreover, *Hooft et al*. [2003] showed that the mantle transition zone is anomalously thin beneath the southwestern archipelago, and they attributed this anomaly to elevated temperatures within a hot plume that is upwelling from depths greater than 410 km. Tomographic analysis of surface wave data and a joint analysis of body and surface wave data show a low-velocity anomaly above the anomalously thin transition zone that is consistent with plume upwelling [*Villagómez et al*., 2007, 2014] (Figure 5). The low-velocity anomaly between 200 and 300 km depth is located south of Isabela and is not deflected eastward in the direction of plate motion (Figures 1 and 5). Between 200 and 100 km depth, substantially deeper than the base of the thermal lithosphere, the low-velocity anomaly is inclined toward the Galápagos Spreading Center (Figure 5a). Tomographic imaging also reveals a high-velocity anomaly in the uppermost mantle that is approximately 80 and 150 km thick in the northern

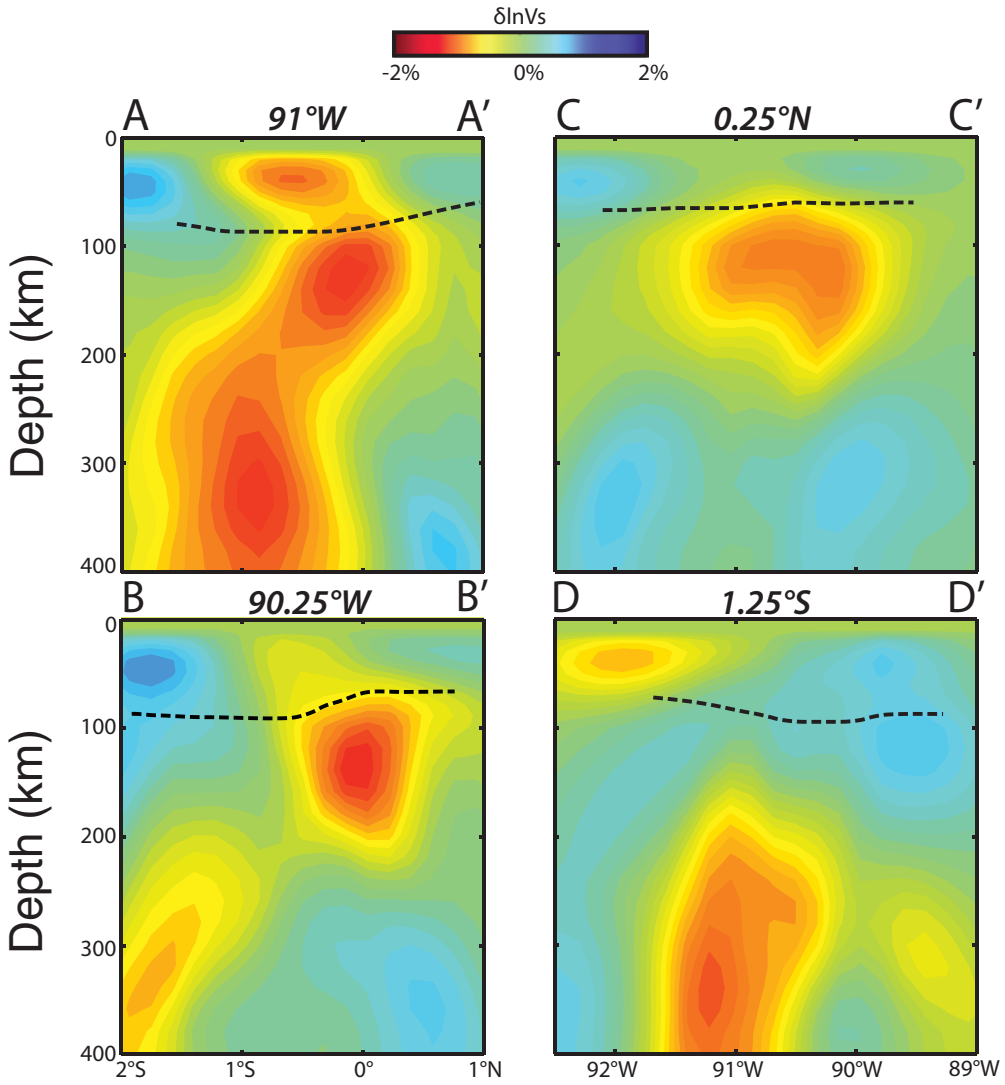

Figure 5. Overlays of the depth of the *G* discontinuity from Figure 2 (dashed lines) on cross sections through the seismic tomographic models of *Villagómez et al.* [2014]. (a, b) Cross sections in the south-to-north direction. (c, d) Cross sections in the west-to-east direction. The locations of the cross sections are shown in Figure 1. The seismic velocity anomalies are plotted as percent change relative to a one-dimensional velocity model that corresponds to the 1350°C adiabat (Figure 11 of *Villagómez et al.* [2007]).

and southern archipelago, respectively; this feature is both thicker and more prominent in the southeastern archipelago. *Villagómez et al.* [2007, 2014] attributed this feature, which we term the "high-velocity lid," to chemical depletion and dehydration associated with melt removal. Above the inferred plume and within the high-velocity lid, an approximately 100-km-wide region of reduced velocity is observed at ~40 km depth (Figure 5a); this feature has been attributed to decompression melting of upwelling mantle [*Villagómez et al.*, 2007, 2014].

Beneath most of the archipelago the depth of the G discontinuity lies within or near the base of the high-velocity lid (Figure 5). Moreover, as the Nazca plate moves to the east [*Gripp and Gordon*, 2002] over the Galápagos plume (near 91°W), both the depth of the G discontinuity and the thickness of the high-velocity lid increase substantially (Figures 3a and 5). This increase in thickness of the high-velocity lid is clear in the difference between the southern ends of profiles A-A′ and B-B′ (Figures 5a and 5b) and on the eastern end of profile D-D′ (Figure 5d). In the northern archipelago, the G discontinuity and the base of the high-velocity lid are shallower and appear at approximately the same depth (north ends of profiles A-A′ and B-B′, Figures 5a and 5b, and profile C-C′, Figure 5c). Exceptions are (i) the presence of the G discontinuity beneath the

shallow low-velocity anomaly that overlies the plume (Figure 5a, profile A-A'), and (ii) the presence of the G discontinuity shallower than high-velocity anomalies that extend to the bottom of the tomographic model in the southeastern corner of the study area (Figure 5d, profile D-D'), a pattern that may be the result of downwelling along the margins of the archipelago [*Villagómez et al*., 2014].

4.2. The G Discontinuity Marks the Base of Fully Dehydrated Mantle

Building on the interpretation of *Villagómez et al*. [2007, 2014], we propose that the observed G discontinuity marks the base of a depleted and dehydrated residuum and is a consequence of the removal of hydrogen from olivine by dehydration melting. A thermal origin for the G discontinuity can be rejected because of its depth and spatial pattern. First, plate-cooling models predict that the thermal lithosphere is only 30–40 km thick beneath the archipelago [*Turcotte and Schubert*, 2002], values that are approximately half of the observed depth of the G discontinuity (70–90 km). Second, for a thermally controlled boundary, the depth to the G discontinuity is expected to have decreased where the plate has passed over the plume thermal anomaly—a prediction opposite to the observed pattern (Figure 3a).

The observed depth of the G discontinuity and its increase to the east of the Galápagos plume forms the basis for our interpretation of this boundary as the base of a depleted and dehydrated layer (Figure 3a). The observed depths of the G discontinuity are in general agreement with laboratory predictions of the thickness of a layer of depleted and dehydrated residuum beneath oceanic crust (60–100 km depth) [e.g., *Hirth and Kohlstedt*, 1996; *Phipps Morgan*, 1997, *Karato and Jung*, 1998]. Furthermore, given the eastward motion of the Nazca plate in the hotspot reference frame [*Gripp and Gordon*, 2002], we infer that the depth of the G discontinuity increases when the Nazca plate moves over the Galápagos plume. This increase in discontinuity depth corresponds to predictions that elevated plume temperatures will cause melt extraction and dehydration of the mantle to greater depths, producing a thicker layer of high-viscosity and high-seismic velocities.

In the region of the present Galápagos plume (southern Isabela), the depth of the G discontinuity (82 ± 10 km) appears to be intermediate between the depths beneath the southeastern archipelago and surrounding portions of the archipelago (Figure 4). We consider two possible interpretations for this apparent depth. The intermediate depth (82 ± 10 km) could be the result of limited spatial resolution of a more abrupt change with horizontal distance. Alternatively, a *G* discontinuity at this intermediate depth is consistent with a 91-km-deep discontinuity that is in the process of being formed over the mantle plume. This view implies either that the discontinuity forms gradually as it deepens from 72 km depth to 91 km depth over a horizontal distance of approximately 100 km, or that the locally high melt flux directly above the plume stem alters the seismic structure of the overlying mantle.

4.3. Potential Temperature of the Plume and Surrounding Mantle

Our interpretation of the G discontinuity as the base of a depleted and dehydrated layer is consistent with the predicted depth of the solidus for anhydrous mantle material and independent estimates of mantle temperature at both the Galápagos Spreading Center (Table 1) and the Galápagos plume (Table 2). The G discontinuity is at 91 ± 8 km depth only where the plate has passed over the inferred center of the upwelling plume, located beneath southern Isabela. This outcome suggests that the G discontinuity depth of 72 ± 5 km in the surrounding region was formed by melting during upwelling beneath the Galápagos Spreading Center away from the direct influence of the upwelling plume stem. Our interpretation that the anhydrous solidus is at 72 ± 5 km depth corresponds to a potential temperature of 1387 ± 25°C (on the basis of the solidus curve of *Herzberg et al*. [2000]). This value is consistent with previous estimates of a 20°–50°C excess potential temperature at the Galápagos Spreading Center near the archipelago (Table 1 and references therein), relative to a reference mantle potential temperature of 1350°C for parts of the Galápagos Spreading Center not influenced by the plume [*Asimow and Langmuir*, 2003].

In the southeastern archipelago, the depth of the G discontinuity at 91 ± 8 km implies a potential temperature at the time of formation of 1465 ± 30°C [*Herzberg et al*., 2000]. Relative to a reference mantle potential temperature of 1350°C, this figure gives an excess potential temperature of 115 ± 30°C for the Galápagos plume. This result agrees well with previously published estimates of approximately 75°–200°C for the excess temperature of the Galápagos plume (Table 2 and references therein).

Table 1. Estimates for the Excess Temperature of the Galápagos Spreading Center Near 91° W

Study	Excess Temperature (°C)	Method
Ito and Lin [1995]	50 ± 25	From modeling of crustal thickness and gravity
Detrick et al. [2002]	30	From crustal thickness
Asimow and Langmuir [2003]	45	From modeling of major and trace elements of basalts and crustal thickness
Cushman et al. [2004]	20	From modeling of glass chemistry
Ingle et al. [2010]	30	From modeling of trace elements and isotopic data
This study	37[a] ± 25	From an interpretation of the G seismic discontinuity

[a]Excess temperature was calculated relative to a reference mantle temperature of 1350°C, as inferred along the Galápagos Spreading Center between 85° and 87° W [*Asimow and Langmuir*, 2003].

4.4. A Scenario for Mantle Melting and Seismic Velocity Changes

We propose that mantle upwelling through the depth interval of volatile-induced melting results in a progressive increase in seismic velocity with decreasing depth. When upwelling mantle material subsequently crosses the anhydrous solidus at shallower depth, an abrupt increase in seismic velocity results (Figure 6a–6c). This hypothesis provides a consistent explanation of both our results and previous seismic and geochemical studies in the Galápagos Archipelago. By this view, where the plate has been influenced by the plume, volatile-enhanced melting is more substantial, resulting in (i) a deeper G discontinuity and thicker high-velocity lid, and (ii) a high-velocity lid that extends to greater depth than the G discontinuity (Figure 6d).

We illustrate the viscosity and velocity structures that will result from melt extraction and H_2O removal over a mantle plume in Figure 6. At depths greater than that at which the anhydrous solidus is reached, a small amount of melt is produced because of the presence of volatiles [*Hirschmann*, 2010, and references therein]. Both CO_2 and H_2O induce melting at temperatures below the anhydrous solidus [*Dasgupta et al.*, 2007]. Upwelling through the depth interval between the solidus temperatures for volatile-bearing and anhydrous mantle material produces a small amount of melt per upward displacement, and the mantle progressively dehydrates (Figure 6b), which increases the viscosity [*Karato*, 1986; *Hirth and Kohlstedt*, 1996; *Phipps Morgan*, 1997] and seismic velocity [*Karato and Jung*, 1998; *Karato*, 2012] of the material (Figure 6c).

When the upwelling mantle reaches the anhydrous solidus, melt production greatly increases [*Hirth and Kohlstedt*, 1996], and the remaining water is removed from olivine, creating a pronounced upward increase in viscosity and seismic velocity that is sharp relative to the seismic wavelength (Figure 6). Whereas the removal of water at the anhydrous solidus can be more pronounced in fractional than batch melting [*Hirschmann*, 2010], melting models that do not yield an abrupt increase in melt production at the anhydrous solidus still predict that all of the water is effectively removed from the mantle at similar depths [e.g., *Asimow et al.*, 2004].

Although the amount of water that remains before the upwelling mantle reaches the anhydrous solidus is likely small [*Hirth and Kohlstedt*, 1996, Figure 4], the physical properties of olivine are predicted to change

Table 2. Estimates for the Excess Temperature of the Galápagos Plume

Study	Excess Temperature (°C)	Method
Schilling [1991]	214 ± 50	From modeling of the elevation and geographical extent of geochemical anomalies at spreading centers that interact with mantle plumes.
Ito and Lin [1995]	200	From scaling relations between crustal thickness and temperature [*McKenzie*, 1984]
Hooft et al. [2003]	130 ± 60	From mantle transition zone thickness
Herzberg and Gazel [2009]	135[a]	From FeO and MgO contents of primary magmas
Gibson and Geist [2010]	75–100[a]	From variations in rare-earth-element concentrations in lavas at Fernandina (75°C) and Santiago (100°C)
Rychert et al. [2014]	100–200	From an interpretation of a seismic discontinuity as the onset of melting
This study	115[a] ± 30	From an interpretation of the G seismic discontinuity

[a]Excess temperature was calculated relative to a reference mantle temperature of 1350°C, as inferred along the Galápagos Spreading Center between 85° and 87° W [*Asimow and Langmuir*, 2003].

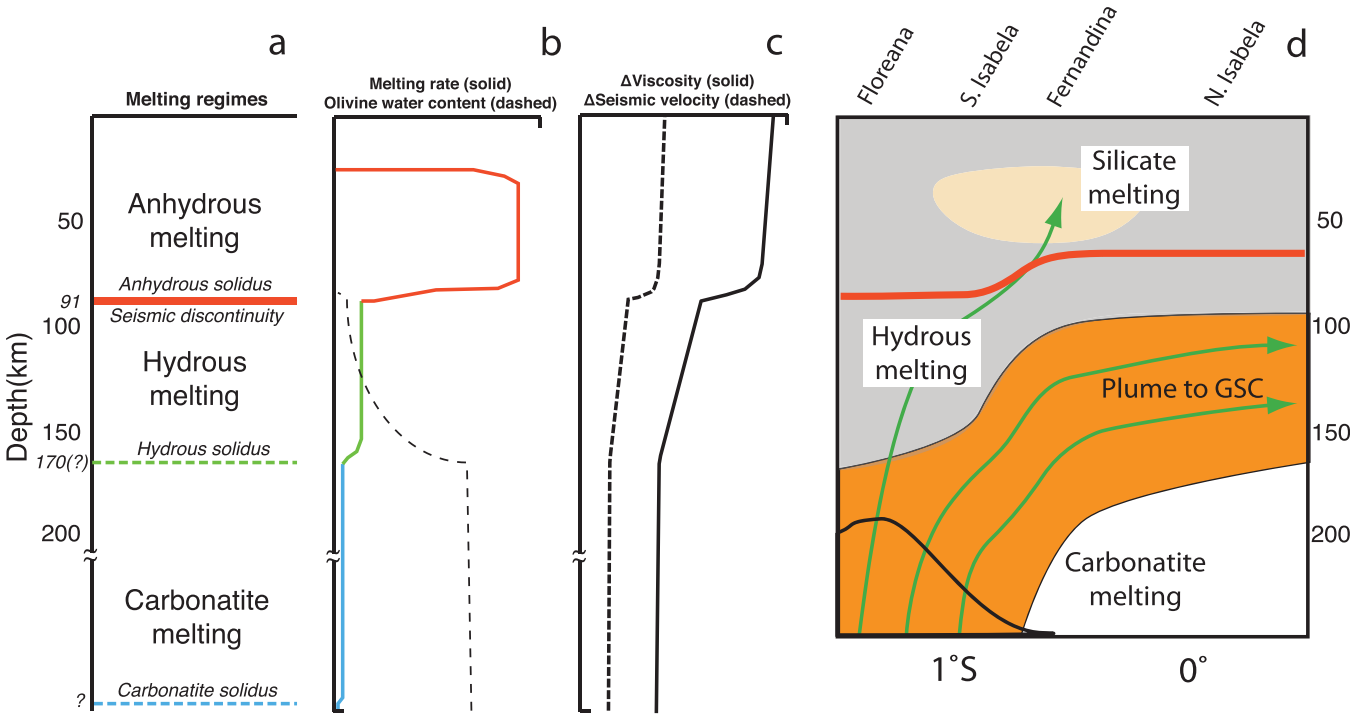

Figure 6. Scenario for mantle melting and its effect on physical properties (cf. Figure 1 of *Choblet and Paramentier* [2001]). (a) Diagram showing the approximate depth extent of the carbonatite, hydrous, and anhydrous melting regimes over the plume. (b) The corresponding melting rate for a given upwelling rate (solid line) and water content of the mantle (dashed line) as functions of depth. (c) Schematic changes in viscosity (solid line) and seismic velocity (dashed line) as functions of depth as a result of dehydration of the upwelling mantle. (d) Schematic cross section at 91°W, modified from *Villagómez et al.* [2014], showing mantle flow and melting processes beneath the Galápagos region. Mantle flow directions are shown in green, the plume in orange, the partially to fully dehydrated volume in gray, the zone of anhydrous silicate melting in light orange, elevated temperature and water content within the plume in black, and the observed G discontinuity and inferred depth of the anhydrous solidus in red.

strongly during the transition from nominally dry to completely dry conditions. Both the viscosity [*Hirth and Kohlstedt*, 1996] and seismic velocity [*Karato and Jung*, 1998; *Karato*, 2012] are reduced by the presence of even a small (less than 100 ppm H/Si) amount of water. Removal of the remaining water thus results in a sharply demarcated, high-viscosity, and high-velocity lid above a region in which velocities and viscosities are lower; in this deeper region, velocity and viscosity gradually increase upward (Figure 6). This model is consistent with positive velocity anomalies that extend deeper than the *G* discontinuity beneath the southeastern archipelago but reach their maximum amplitude above the discontinuity (Figure 5).

The flow pattern of the mantle and the effect of this pattern on melting control the spatial variations in the thickness and internal structure of mantle residuum (Figure 6d). Beneath most of the Galápagos Archipelago, the onset of anhydrous melting in upwelling material at ~72 km is consistent with models of mid-ocean ridge melting at only slightly elevated temperatures beneath the Galápagos Spreading Center as a result of plume-ridge interaction. Within the plume, however, both volatile-enhanced and anhydrous melting begin at greater depths as a result of elevated water content and temperature [*Fisk et al.*, 1982; *Schilling et al.*, 1982; *Detrick et al.*, 2002; *Koleszar et al.*, 2009], so the upward increase in seismic velocity in upwelling material also occurs at greater depths, resulting in a greater depth extent of high-velocity anomalies (to approximately 150 km depth in the southeastern Galápagos, see Figures 5 and 6). Similarly, within the upwelling plume, olivine is dehydrated at greater depths, resulting in the formation of the G discontinuity at 91 ± 8 km.

Results from an earlier receiver function study were also interpreted in the context of the onset of melting and the presence of elevated potential temperatures beneath the Galápagos. *Rychert et al.* [2014] estimated excess potential temperatures beneath the Galápagos by attributing a positive-polarity phase at ~135 km depth to the onset of anhydrous melting at a potential temperature of 1450–1550°C. However, this interpretation requires potential temperatures beneath the entire archipelago that are near, or higher than, the maximum potential temperature of the plume obtained in other studies (Table 2). Instead, we suggest that

our hypothesis, which includes the onset of volatile-enhanced melting, together with mantle potential temperatures that are more consistent with other results, better accounts for the observations of *Rychert et al*. [2014] as well as those of this study. This interpretation requires a water content of 1600–4000 ppm H/Si in the Galápagos mantle at depths greater than the hydrous solidus [*Hirschmann et al*., 2009] for the potential temperatures inferred in our study. If small amounts of the initially hydrous melts are retained in the mantle, a small-amplitude, positive-polarity discontinuity could develop [*Havlin and Parmentier*, 2014]. However, this deep phase, if present, is weak in our receiver functions.

4.5. The Amplitude of the G Discontinuity

The relatively large shear velocity contrast (∼5–11%) across the G discontinuity places bounds on variations in mantle composition, water content, and partial melt content across the boundary. Chemical depletion of the mantle during anhydrous melting is not well understood, and its effect on shear wave velocity has been suggested to range from no significant change [*Schutt and Lesher*, 2006], to a ∼1% increase after 30% melt removal [*Afonso and Schutt*, 2012] to a 2.6% increase with depletion from pyrolite to harzburgite in the spinel stability field [*Matsukage et al*., 2005]. Only if the effect of chemical depletion is near the upper end of these estimates, could it account for a substantial proportion of the observed velocity contrast. We conclude that major-element depletion does not contribute substantially to the amplitude of the seismic discontinuity documented in this study.

We focus instead on the effect of water on the shear quality factor, Q [*Karato and Jung*, 1998]. Motivated by laboratory experiments which suggest that Q decreases with increasing water content in nominally anhydrous minerals [*Jackson et al*., 1992; *Aizawa et al*., 2008], *Karato and Jung* [1998] predicted a reduction in the seismic velocity of hydrated rock that can be described by the absorption band model [*Anderson and Given*, 1982]. The absorption band model predicts that Q decreases with the frequency of a seismic wave as $Q \propto \omega^{-\alpha}$, where ω is the angular frequency and α is a unitless constant that ranges from 0.1 to 0.4 [*Shito et al*., 2004]. In this model, seismic velocity decreases with decreasing Q, and the decrease in velocity is greater at a given Q for smaller values of α. Q would have to lie between ∼20 and ∼40 and be accompanied by a concentration of water of 100 ppm H/Si at depths greater than that of the G discontinuity beneath the southeastern archipelago and the surrounding portions of the archipelago, respectively, to fully account for our velocity contrasts of 11% and 5% (see Appendix A for details). Similar Q values have been reported from other magmatically active regions between 50 and 100 km depth for shear waves at 1 Hz [*Abers et al.,* 2014], but the required values are somewhat lower than estimates for the mantle beneath the East Pacific Rise at similar depths for waves at 10 to 70 s period [*Yang et al*., 2007]. If other factors contribute to the velocity discontinuity in addition to high attenuation as a result of water, Q values beneath the discontinuity could be larger.

An alternative explanation is that the shear velocity contrast at the G discontinuity may also be affected by the presence of melt beneath an interface [*Kawakatsu et al*., 2009; *Schmerr*, 2012]. Melt accumulation may occur in the oceanic asthenosphere between 80 and 100 km depth, because the pressure dependence of the density and viscosity of basaltic melts suggests that melts are neutrally buoyant at these depths [*Sakamaki et al*., 2013]. The effect of accumulated melt on shear velocity depends strongly on the geometry of the melt distribution. Melt retained in organized, cuspate films reduces seismic velocity by 8% for a melt fraction of 1% [*Hammond and Humphries*, 2000]. Models of melt inclusions with large aspect ratios [*Tandon and Weng*, 1984] or of melt segregated into horizontal bands [*Kawakatsu et al*., 2009, and references therein] can account for velocity reductions of ∼6% with melt fractions as low as ∼0.02%. We conclude that partial melt, which could be retained in a range of possible geometries immediately below the G discontinuity, may contribute to the velocity contrast.

Of course, a combination of the above processes is also possible. For instance, if we assume that melt retained in organized cuspate films lowers the shear wave velocity [*Hammond and Humphries*, 2000], a 4% velocity contrast can be generated by a 0.5% contrast in melt fraction across the G discontinuity. If at the same depth 100 ppm H/Si water were removed from subsolidus mantle material with a Q of 50 (see Appendix A), dehydration would contribute another 4% change in velocity. If chemical depletion further increases the velocity above the discontinuity by 1–2%, then the net effect of all three processes is a ∼9–10% contrast in velocity, similar to the observed value beneath the southeastern archipelago.

4.6. The G Discontinuity Is Not the LAB

Many recent studies invoke the explanation that a sharp decrease in seismic velocity with depth in the oceanic upper mantle corresponds to the boundary that separates the mechanically strong, conductively

cooled lithosphere from the convecting asthenosphere [*Fischer et al.,* 2010; *Rychert et al*., 2010; *Kind et al*., 2012]. Three independent arguments indicate that the G discontinuity beneath the Galápagos, in contrast, is not the LAB. First, the seismic discontinuity lies beneath a ~100 km wide region of anomalously low seismic velocities that has been attributed to decompression melting of anhydrous peridotite (see Figures 5 and 6 and the discussion by *Villagómez et al*. [2014]). That the low-velocity anomaly underlies the three most active volcanoes in the archipelago suggests that it is the source region for magmatism. Second, the iron and magnesium contents of young Galápagos lavas, calibrated to the potential temperature and pressure at the point of melt extraction, suggest that primary melt production occurs above the seismic discontinuity. The shallowest melting, inferred from samples throughout the archipelago, occurs at a pressure of 2.0 ± 0.28 GPa, or 60 ± 8 km depth [*Herzberg and Gazel*, 2009]. This depth is 31 ± 11 and 12 ± 9 km shallower than the discontinuity beneath the southeastern archipelago and surrounding parts of the archipelago, respectively. These values suggest that decompression melting, and hence mantle upwelling, continues to depths shallower than the seismic discontinuity. Third, variations in rare-earth-element concentrations in lavas reflect the proportion of melting that occurred in the garnet and spinel stability fields and thus constrain the depth to the top of the melting column. Analyses of rare-earth-element concentrations in Galápagos lavas are also consistent with mantle melting at depths shallower than the observed seismic discontinuity [*Gibson and Geist*, 2010]. The top of the melting column is inferred to reach depths as shallow as 46 km, whereas the G discontinuity is found at 72 and 91 km depth. Because lithosphere, by definition, should not convect upward, the G discontinuity beneath the Galápagos Archipelago is not the LAB.

Mantle upwelling has been inferred to occur above the G discontinuity in other volcanically active settings as well. Beneath Iceland, seismic studies have established an increase in seismic velocity at ~80 km depth, sometimes identified with the LAB [*Kumar et al*., 2005]. However, melting is thought to occur as shallow as 40–50 km depth [*Shen and Forsyth*, 1995], a result consistent with the broad, low-velocity anomalies observed between 50 and 80 km depth [*Li and Detrick*, 2006]. Beneath the High Lava Plains in Oregon, *Till et al*. [2013] inferred that the melting column extends almost to the base of the crust (~35 km depth), consistent with low-shear wave velocity anomalies seen in surface wave tomography [*Wagner et al*, 2012]. In this setting, the LAB had previously been inferred from receiver functions to occur at ~70 km depth [*Li et al*., 2007; *Abt et al*., 2010]. Moreover, a G discontinuity beneath the island of Hawai'i was observed at 110 km depth [*Li et al*., 2004], but the minimum depth of melting inferred from thermobarometric modeling of mafic magma compositions is between 35 and 60 km [*Lee et al*., 2009].

Our results raise an important question. Many recent studies [e.g., *Fischer et al*., 2010; *Kind et al*., 2012, and references therein] have led to the suggestion that the G discontinuity observed in the oceanic upper mantle marks the LAB. We argue that dehydration of the oceanic upper mantle during melting beneath the Galápagos has resulted in a layer of residuum that is not strictly part of the lithosphere, but the residuum is higher in viscosity than the underlying volatile-bearing peridotite [*Hirth and Kohlstedt*, 1996; *Phipps Morgan*, 1997]. This combination of circumstances may apply in other oceanic regions as well. Moreover, this residuum need not be homogeneous but can be variable in its water content and thus its rheologic and seismic properties. Under certain conditions, the residuum can move with oceanic lithosphere, relax [*Phipps Morgan et al*., 1995], or even upwell and continue melting, as it likely does beneath the Galápagos Archipelago and as it must do beneath spreading centers [e.g., *Ito et al*., 1999].

5. Conclusions

We have documented a seismic discontinuity, identified as the G discontinuity, in the mantle beneath the Galápagos Archipelago on the basis of *S*-to-*p* conversions mapped with receiver functions. The discontinuity is deeper in the southeastern archipelago than in the surrounding region, 91 ± 8 versus 72 ± 5 km, respectively. We attribute the seismic discontinuity to the base of a dehydrated and depleted layer that corresponds to the deepest extent of anhydrous melting. The 72-km-deep discontinuity formed at or near the Galápagos Spreading Center, whereas the 91-km-deep discontinuity beneath the southeastern archipelago is the result of the Nazca plate having moved over an upwelling mantle plume with an excess potential temperature of 115 ± 30°C. That the observed change in shear velocity across the G discontinuity is larger beneath the southeastern Galápagos than in the surrounding region, 11% versus 5%, could result from some combination of chemical depletion, dehydration of olivine, and a contrast in partial melt fraction.

The G discontinuity lies within a high-velocity lid imaged with seismic tomography. We interpret this geometry as indicating that below the discontinuity, between the depths at which the solidus temperatures for volatile-bearing and anhydrous mantle material are reached, the upwelling mantle is partially dehydrated and viscosity and seismic velocity gradually increase upward. At the anhydrous solidus, the remaining water is removed, creating a sharp increase in viscosity and seismic velocity with further ascent that results in the observed discontinuity. Results from seismic tomography and geochemistry require that mantle upwelling and partial melting continue above the G discontinuity and within the dehydrated and depleted layer. These observations are inconsistent with the assumption, commonly made on the basis of seismic observations in other regions, that such a discontinuity represents the base of the rigid lithosphere, or the LAB. That the G discontinuity is not the lithosphere-asthenosphere boundary in the Galápagos raises the question of the extent to which the association between this seismic discontinuity and the LAB is generally applicable.

Appendix A: Effect of Dehydration on Seismic Velocity

We used the model of *Karato and Jung* [1998] to estimate the effect of dehydration on seismic velocity. In this model, the concentration of water in mantle minerals (primarily olivine) has almost no effect on the elastic behavior of the mantle. The water content of the mantle affects only anelastic behavior, described by the shear wave quality factor Q. Laboratory studies strongly suggest, but have not conclusively demonstrated, that small amounts of dissolved water in nominally anhydrous minerals (even less than 100 ppm H/Si) can reduce Q; conversely, removing water from these minerals increases Q. Here, we summarize this model and give values that would be necessary to explain the amplitude of the G discontinuity beneath the Galápagos.

In an anelastic material, energy is lost during deformation, which attenuates seismic waves. The degree of anelasticity is characterized by Q; the higher the Q, the less energy is lost. Q depends strongly on the frequency of a seismic wave. Beneath young oceanic lithosphere [*Jackson and Faul*, 2010], Q is predicted to depend on ω as $Q \propto \omega^{-\alpha}$, where ω is the angular frequency and α is a dimensionless constant called the frequency dependence that varies in the Earth from 0.1 to 0.4. This model for Q is known as the absorption band model [*Anderson and Given*, 1982].

Low-Q materials are not only attenuating, they have lower seismic velocity. The fractional reduction in shear velocity relative to the perfectly elastic velocity (V_o) is given approximately by

$$\frac{\Delta V}{V_o} = \frac{1}{2}\cot\left(\frac{\pi\alpha}{2}\right)Q^{-1} \tag{A1}$$

The reduction in shear velocity, ΔV, is therefore greater when Q is lower or when α is lower (i.e., when a material is more attenuating or when Q is less dependent on frequency). Removing water from the mantle increases Q and increases the shear velocity. By this means, a dehydration boundary can create a seismic discontinuity.

Because a rigorously derived relation between Q and water content has not been established, we use the approximation of *Karato and Jung* [1998] by which Q depends on the concentration of water, $C_{OH,}$ according to

$$Q^{-1} \propto C_{OH}^{\alpha} \tag{A2}$$

To derive (A2), we assume that the only term in the model of *Karato and Jung* [1998] that changes when the upwelling mantle crosses the solidus is C_{OH}. We model the effect of water on seismic velocity through the effect of water on Q for an assumed value of Q at temperatures below the solidus. A change in water concentration by a factor of 100 would mean a change in Q of 100^{α}, or 1.5–4 for an α value of 0.1–0.3, respectively. Note that Q changes more for greater α, but it affects the seismic velocity more strongly for smaller α because of the cotangent term in equation (A1).

We cannot rigorously constrain the concentration of water or Q at different depths beneath the Galápagos, but we can calculate the combination of Q, C_{OH}, and α that could give a sufficiently large velocity contrast to account for at least part of our observations. First, we note that laboratory studies suggest that α can be $\sim$0.1 in partially molten rocks [*Faul et al.*, 2004] and 0.1 represents the lower end of the observed values of

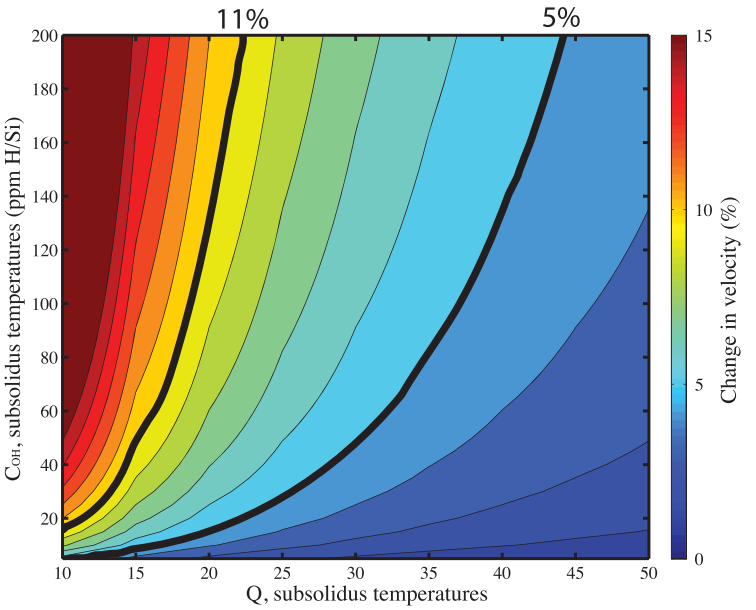

Figure A1. Calculated change in shear velocity at the anhydrous solidus dehydration boundary as a result of anelasticity. Bold contours indicate the inferred velocity contrasts beneath the southeastern archipelago (11%) and surrounding region (5%).

α [*Shito et al.*, 2004]. We fixed the value of α at 0.1 to maximize the effect of water on seismic velocity. Second, we assume, following *Karato and Jung* [1998], that at a C_{OH} of 1 ppm H/Si the behavior of a nominally anhydrous mineral is the same as under fully anhydrous conditions. We consider dehydration, then, to be equivalent to the reduction of C_{OH} to 1 ppm H/Si.

We used equations (A1) and (A2) to calculate the shear velocity change induced by dehydration across the anhydrous solidus for different initial values of Q and C_{OH}, as shown in Figure A1. Our observed velocity contrasts of 5% and 11% are both within the parameter space shown. We note two important issues. First, the concentration of water at depths greater than that at which the temperature is at the anhydrous solidus is not the concentration of water in normal mantle. Rather, it is the concentration of water that remains after the upwelling mantle has passed through the volatile-enhanced melting regime. Although the Galápagos plume at sufficient depth may have a fairly high concentration of water [*Koleszar et al.*, 2009], the majority of the water will have been removed before the upwelling material reaches the depth at which the temperature is at the anhydrous solidus [*Hirth and Kohlstedt*, 1996]. Second, the values of Q necessary to explain fully the discontinuities are low, 20–35 for 100 ppm H/Si. Had we assumed a larger value for α, the required Q values would be even lower. For comparison, Q beneath the East Pacific Rise is as low as 50 between 50 and 100 km depth for shear wave periods betwen 10 and 70 s [*Yang et al.*, 2007]. However, values of Q similar to those required to match the results for the Galápagos region are observed in magmatically active areas between 50 and 100 km depth for energy at 1 Hz [*Abers et al.*, 2014]. Another possible explanation of our observations is that the amplitude of the G discontinuity is not controlled solely by dehydration, but by a combination of factors, including depletion by melt extraction and a contrast in retained melt fraction.

Acknowledgments
We thank Minard Hall of the Instituto Geofísico at the Escuela Politécnica Nacional in Quito, the Charles Darwin Research Station, and the Parque Nacional Galápagos for logistical support and assistance in the field. We thank Ulrich Faul, Garrett Ito, and an anonymous reviewer for their insightful comments, which helped improve this manuscript. This research was supported by the National Science Foundation under grants OCE-9908695, OCE-0221549, and EAR-0651123 to the University of Oregon, OCE-0221634 to the Carnegie Institution of Washington, and EAR-11452711 to the University of Idaho. The seismic data used in this paper are available from the Data Management Center of the Incorporated Research Institutions for Seismology under the network code YH.

References

Abers, G. A., K. M. Fischer, G. Hirth, D. A. Wiens, T. Plank, B. K. Holtzman, C. McCarthy, and E. Gazel (2014), Reconciling mantle attenuation-temperature relationships from seismology, petrology, and laboratory measurements, *Geochem. Geophys. Geosyst.*, *15*, 3521–3542, doi:10.1002/2014GC005444.

Abt, D. L., K. M. Fischer, S. W. French, H. A. Ford, H. Yuan, and B. Romanowicz (2010), North American lithospheric discontinuity structure imaged by Ps and Sp receiver functions, *J. Geophys. Res.*, *115*, B09301, doi:10.1029/2009JB006914.

Afonso, J. C., and D. L. Schutt (2012), The effects of polybaric partial melting on density and seismic velocities of mantle restites, *Lithos*, *134*, 289–303, doi:10.1016/j.lithos.2012.01.009.

Aizawa, Y., A. Barnhoorn, U. H. Faul, J. D. F. Gerald, I. Jackson, and I. Kovács (2008), Seismic properties of Anita Bay dunite: An exploratory study of the influence of water, *J. Petrol.*, *49*, 841–855, doi:10.1093/petrology/egn007.

Anderson, D. L., and J. W. Given (1982), Absorption band Q model for the Earth, *J. Geophys. Res.*, *87*, 3893–3904, doi:10.1029/JB087iB05p03893.

Asimow, P. D., and C. H. Langmuir (2003), The importance of water to oceanic mantle melting regimes, *Nature*, *421*, 815–820, doi:10.1038/nature01429.
Asimow, P. D., J. E. Dixon, and C. H. Langmuir (2004), A hydrous melting and fractionation model for mid-ocean ridge basalts: Application to the Mid-Atlantic Ridge near the Azores, *Geochem. Geophys. Geosyst.*, *5*, Q01E16, doi:10.1029/2003GC000568.
Bagley, B., and J. Revenaugh (2008), Upper mantle seismic shear discontinuities of the Pacific, *J. Geophys. Res.*, *113*, B12301, doi:10.1029/2008JB005692.
Barckhausen, U., C. R. Ranero, R. von Huene, S. C. Cande, and H. A. Roeser (2001), Revised tectonic boundaries in the Cocos plate off Costa Rica: Implications for the segmentation of the convergent margin and for plate tectonic models, *J. Geophys. Res.*, *106*, 19,207–19,220, doi:10.1029/2001JB000238.
Beghein, C., K. Yuan, N. Schmerr, and Z. Xing (2014), Changes in seismic anisotropy shed light on the nature of the Gutenberg discontinuity, *Science*, *343*, 1237–1240, doi:10.1126/science.1246724.
Brocher, T. M. (2005), Empirical relations between elastic wavespeeds and density in the Earth's crust, *Bull. Seismol. Soc. Am.*, *95*, 2081–2092, doi:10.1785/0120050077.
Choblet, G., and E. M. Parmentier (2001), Mantle upwelling and melting beneath slow spreading centers: Effects of variable rheology and melt productivity, *Earth Planet. Sci. Lett.*, *184*, 589–604, doi:10.1016/S0012–821X(00)00330-7.
Collins, J. A., F. L. Verson, J. A. Orcutt, and R. A. Stephen (2002), Upper mantle structure beneath the Hawaiian swell: Constraints from the ocean seismic network pilot experiment, *Geophys. Res. Lett.*, *29*, 1522, doi:10.1029/2001GL013302.
Cushman, B., J. Sinton, G. Ito, and J. E. Dixon (2004), Glass compositions, plume-ridge interaction, and hydrous melting along the Galápagos Spreading Center, *Geochem. Geophys. Geosyst.*, *5*, Q08E17, doi:10.1029/2004GC000709.
Dasgupta, R., M. M. Hirschmann, and N. D. Smith (2007), Water follows carbon: CO_2 incites deep silicate melting and dehydration beneath mid-ocean ridges, *Geology*, *35*, 135–138, doi:10.1130/G22856A.1.
Detrick, R. S., and S. T. Crough (1978), Island subsidence, hot spots, and lithospheric thinning, *J. Geophys. Res.*, *83*, 1236–1244, doi:10.1029/JB083iB03p01236.
Detrick, R. S., J. M. Sinton, G. Ito, J. P. Canales, M. Behn, T. Blacic, B. Cushman, J. E. Dixon, D. W. Graham, and J. J. Mahoney (2002), Correlated geophysical, geochemical, and volcanological manifestations of plume-ridge interaction along the Galápagos Spreading Center, *Geochem. Geophys. Geosyst.*, *3*, 8501, doi:10.1029/2002GC000350.
Dueker, K. G., and A. F. Sheehan (1998), Mantle discontinuity structure beneath the Colorado Rocky Mountains and High Plains, *J. Geophys. Res.*, *103*, 7153–7169, doi:10.1029/97JB03509.
Faul, U. H., and I. Jackson (2005), The seismological signature of temperature and grain size variations in the upper mantle, *Earth Planet. Sci. Lett.*, *234*, 119–134, doi:10.1016/j.epsl.2005.02.008.
Faul, U. H., J. D. Fitzgerald, and I. Jackson (2004), Shear wave attenuation and dispersion in melt-bearing olivine polycrystals: 2. Microstructural interpretation and seismological implications, *J. Geophys. Res.*, *109*, B06202, doi:10.1029/2003JB002407.
Fischer, K. M., H. A. Ford, D. L. Abt, and C. A. Rychert (2010), The lithosphere-asthenosphere boundary, *Annu. Rev. Earth Planet. Sci.*, *38*, 551–575, doi:10.1146/annurev-earth-040809–152438.
Fisk, M. R., A. E. Bence, and J. G. Schilling (1982), Major element chemistry of Galápagos rift zone magmas and their phenocrysts, *Earth Planet. Sci. Lett.*, *61*, 171–189, doi:10.1016/0012–821X(82)90050-4.
Gaherty, J. B., T. H. Jordan, and L. S. Gee (1996), Seismic structure of the upper mantle in a central Pacific corridor, *J. Geophys. Res.*, *101*, 22,291–22,309, doi:10.1029/96JB01882.
Gaherty, J., M. Kato, and T. H. Jordan (1999), Seismological structure of the upper mantle: A regional comparison of seismic layering, *Phys. Earth Planet. Inter.*, *110*, 21–41, doi:10.1016/S0031–9201(98)00132-0.
Gibson, S. A., and D. Geist (2010), Geochemical and geophysical estimates of lithospheric thickness variation beneath Galápagos, *Earth Planet. Sci. Lett.*, *300*, 275–286, doi:10.1016/j.epsl.2010.10.002.
Graham, D. W., D. M. Christie, K. S. Harpp, and J. E. Lupton (1993), Mantle plume helium in submarine basalts from the Galápagos platform, *Science*, *262*, 2023–2026, doi:10.1126/science.262.5142.2023.
Gripp, A. E., and R. G. Gordon (2002), Young tracks of hotspots and current plate velocities, *Geophys. J. Int.*, *150*, 321–361, doi:10.1046/j.1365-246X.2002.01627.x.
Gutenberg, B. (1948), On the relatively low wave velocity at depth of about 80 kilometers, *Bull. Seismol. Soc. Am.*, *38*, 121–147.
Hall, P. S., and C. Kincaid (2003), Melting, dehydration, and the dynamics of off-axis plume-ridge interaction, *Geochem. Geophys. Geosyst.*, *4*, 8510, doi:10.1029/2003GC000567.
Hammond, W. C., and E. D. Humphreys (2000), Upper mantle seismic wave velocity: Effects of realistic partial melt geometries, *J. Geophys. Res.*, *105*, 10,975–10,986, doi:10.1029/2000JB900041.
Hansen, S., and K. Dueker (2009), P-and S-wave receiver function images of crustal imbrication beneath the Cheyenne Belt in southeast Wyoming, *Bull. Seismol. Soc. Am.*, *99*, 1953–1961, doi:10.1785/0120080168.
Harpp, K. S., and W. M. White (2001), Tracing a mantle plume: Isotopic and trace element variations of Galápagos seamounts, *Geochem. Geophys. Geosyst.*, *2*, 1042, doi:10.1029/2000GC000137.
Havlin, C., and E. M. Parmentier (2014), Implications for melt transport and source heterogeneity in upwelling mantle from the magnitude of S_P converted phases generated at the onset of melting, *Geophys. Res. Lett.*, *34*, 5444–5450, doi:10.1002/2014GL060890.
Heit, B., F. Sodoudi, X. Yuan, M. Bianchi, and R. Kind (2007), An S receiver function analysis of the lithospheric structure in South America, *Geophys. Res. Lett.*, *34*, L14307, doi:10.1029/2007GL030317.
Helffrich, G. (2006), Extended-time multitaper frequency domain cross-correlation receiver-function estimation, *Bull. Seismol. Soc. Am.*, *96*, 344–347, doi:10.1785/0120050098.
Herzberg, C., and E. Gazel (2009), Petrological evidence for secular cooling in mantle plumes, *Nature*, *458*, 619–622, doi:10.1038/nature07857.
Herzberg, C., P. Raterron, and J. Zhang (2000), New experimental observations on the anhydrous solidus for peridotite KLB-1, *Geochem. Geophys. Geosyst.*, *1*, 1051, doi:10.1029/2000GC000089.
Hey, R., and P. Vogt (1977), Spreading-center jumps and sub-axial asthenosphere flow near the Galápagos hotspot, *Tectonophysics*, *37*, 41–52, doi:10.1016/0040–1951(77)90038-5.
Hirschmann, M. M. (2010), Partial melt in the oceanic low velocity zone, *Phys. Earth Planet. Inter.*, *179*, 60–71, doi:10.1016/j.pepi.2009.12.003.
Hirschmann, M. M., T. Tenner, C. Aubaud, and A. C. Withers (2009), Dehydration melting of nominally anhydrous mantle: The primacy of partitioning, *Phys. Earth Planet. Inter.*, *176*, 54–68, doi:10.1016/j.pepi.2009.04.001.
Hirth, G., and D. L. Kohlstedt (1996), Water in the oceanic upper mantle: Implications for rheology, melt extraction and the evolution of the lithosphere, *Earth Planet. Sci. Lett.*, *144*, 93–108, doi:10.1016/0012–821X(96)00154-9.

Hooft, E. E., D. R. Toomey, and S. C. Solomon (2003), Anomalously thin transition zone beneath the Galápagos hotspot, *Earth Planet. Sci. Lett.*, *216*, 55–64, doi:10.1016/S0012–821X(03)00517-X.
Ingle, S., G. Ito, J. J. Mahoney, W. Chazey III, J. Sinton, M. Rotella, and D. M. Christie (2010), Mechanisms of geochemical and geophysical variations along the western Galápagos Spreading Center, *Geochem. Geophys. Geosyst.*, *11*, Q04003, doi:10.1029/2009GC002694.
Ito, G., and J. Lin (1995), Mantle temperature anomalies along the past and paleoaxes of the Galápagos spreading center as inferred from gravity analyses, *J. Geophys. Res.*, *100*, 3733–3745.
Ito, G., Y. Shen, G. Hirth, and C. J. Wolfe (1999), Mantle flow, melting, and dehydration of the Iceland mantle plume, *Earth Planet. Sci. Lett.*, *1*, 81–96, doi:10.1016/S0012-821X(98)00216-7.
Jackson, I., and U. H. Faul (2010), Grainsize-sensitive viscoelastic relaxation in olivine: Towards a robust laboratory-based model for seismological application, *Phys. Earth Planet. Inter.*, *183*, 151–163, doi:10.1016/j.epsl.2005.02.008.
Jackson, I., M. S. Paterson, and J. D. Fitz Gerald (1992), Seismic wave dispersion and attenuation in Åheim dunite: An experimental study, *Geophys. J. Int.*, *108*, 517–534, doi:10.1111/j.1365-246X.1992.tb04633.x.
Karato, S. (1986), Does partial melting reduce the creep strength of the upper mantle?, *Nature*, *319*, 309–310, doi:10.1038/319309a0.
Karato, S.-I. (2012), On the origin of the asthenosphere, *Earth Planet. Sci. Lett.*, *321*, 95–103, doi:10.1016/j.epsl.2012.01.001.
Karato, S.-I. (2014), Does partial melting explain geophysical anomalies? *Phys. Earth Planet. Inter.*, *228*, 300–306, doi:10.1016/j.pepi.2013.08.006.
Karato, S.-I., and H. Jung (1998), Water, partial melting and the origin of the seismic low velocity and high attenuation zone in the upper mantle, *Earth Planet. Sci. Lett.*, *157*, 193–207, doi:10.1016/S0012–821X(98)00034-X.
Kawakatsu, H., P. Kumar, Y. Takei, M. Shinohara, T. Kanazawa, E. Araki, and K. Suyehiro (2009), Seismic evidence for sharp lithosphere-asthenosphere boundaries of oceanic plates, *Science*, *324*, 499–502, doi:10.1126/science.1169499.
Kind, R., X. Yuan, and P. Kumar (2012), Seismic receiver functions and the lithosphere–asthenosphere boundary, *Tectonophysics*, *536–537*, 25–43, doi:10.1016/j.tecto.2012.03.005.
Koleszar, A. M., A. E. Saal, E. H. Hauri, A. N. Nagle, Y. Liang, M. D. Kurz (2009), The volatile contents of the Galápagos plume; evidence for H_2O and F open system behavior in melt inclusions, *Earth Planet. Sci. Lett.*, *287*, 442–452, doi:10.1016/j.epsl.2009.08.029.
Kumar, P., and H. Kawakatsu (2011), Imaging the seismic lithosphere-asthenosphere boundary of the oceanic plate, *Geochem. Geophys. Geosyst.*, *12*, Q01006, doi:10.1029/2010GC003358.
Kumar, P., R. Kind, W. Hanka, K. Wylegalla, C. Reigber, X. Yuan, I. Woelbern, P. Schwintzer, K. Fleming, and T. Dahl-Jensen (2005), The lithosphere–asthenosphere boundary in the North-West Atlantic region, *Earth Planet. Sci. Lett.*, *236*, 249–257, doi:10.1016/j.epsl.2005.05.029.
Kumar, P., X. Yuan, M. R. Kumar, R. Kind, X. Li, and R. K. Chadha (2007), The rapid drift of the Indian tectonic plate, *Nature*, *449*, 894–897, doi:10.1038/nature06214.
Kurz, M. D., and D. Geist (1999), Dynamics of the Galápagos hotspot from helium isotope geochemistry, *Geochim. Cosmochim. Acta*, *63*, 4139–4156, doi:10.1016/S0016–7037(99)00314-2.
Lee, C. A., P. Luffi, T. Plank, H. Dalton, and W. P. Leeman (2009), Constrains on the depths and temperatures of basaltic magma generation on Earth and other terrestrial planets using new thermobarometers for mafic magma, *Earth Planet. Sci. Lett.*, *279*, 20–33, doi:10.1016/j.epsl.2008.12.020.
Levin, V., and J. Park (1998), P-SH conversions in layered media with hexagonally symmetric anisotropy: A cookbook, *Pure Appl. Geophys.*, *151*, 669–697, doi:10.1007/s000240050136.
Li., A., and R. S. Detrick (2006), Seismic structure of Iceland from Rayleigh wave inversions and geodynamic implications, *Earth Planet. Sci. Lett.*, *241*, 901–912, doi:10.1016/j.epsl.2005.10.031.
Li, X., R. Kind, X. Yuan, I. Wölbern, and W. Hanka (2004), Rejuvenation of the lithosphere by the Hawaiian plume, *Nature*, *427*, 827–829, doi:10.1038/nature02349.
Li, X., X. Yuan, and R. Kind (2007), The lithosphere-asthenosphere boundary beneath the western United States, *Geophys. J. Int.*, *170*, 700–710, doi:10.1111/j.1365-246X.2007.03428.x.
Lodge, A., and G. Helffrich (2006), Depleted swell root beneath the Cape Verde Islands, *Geology*, *34*, 449–452, doi:10.1130/G22030.1.
Matsukage, K. N., Y. Nishihara, and S.-I. Karato (2005), Seismological signature of chemical differentiation of Earth's upper mantle, *J. Geophys. Res.*, *110*, B12305, doi:10.1029/2004JB003504.
McKenzie, D. (1984), The generation and compaction of partially molten rock, *J. Petrol.*, *25*, 713–765, doi:10.1093/petrology/25.3.713.
Mittelstaedt, E., G. Ito, and J. van Hunen (2011), Repeat ridge jumps associated with plume-ridge interaction, melt transport, and ridge migration, *J. Geophys. Res.*, *116*, B01102, doi:10.1029/2010JB007504.
Park, J. (1996), Surface waves in layered anisotropic structures, *Geophys. J. Int.*, *126*, 173–183, doi:10.1111/j.1365-246X.1996.tb05276.x.
Park, J., and V. Levin (2000), Receiver functions from multiple-taper spectral correlation estimates, *Bull. Seismol. Soc. Am.*, *90*, 1507–1520, doi:10.1785/0119990122.
Park, J., C. R. Lindberg, and F. L. Vernon (1987), Multitaper spectral analysis of high-frequency seismograms, *J. Geophys. Res.*, *92*, 12,675–12,684, doi:10.1029/JB092iB12p12675.
Parsons, B., and D. McKenzie (1978), Mantle convection and the thermal structure of the plates, *J. Geophys. Res.*, *83*, 4485–4496, doi:10.1029/JB083iB09p04485.
Phipps Morgan, J. (1997), The generation of a compositional lithosphere by mid-ocean ridge melting and its effect on subsequent off-axis hotspot upwelling and melting, *Earth Planet. Sci. Lett.*, *146*, 213–232, doi:10.1016/S0012–821X(96)00207-5.
Phipps Morgan, J., W. J. Morgan, and E. Price (1995), Hotspot melting generates both hotspot volcanism and a hotspot swell?, *J. Geophys. Res.*, *100*, 8045–8062, doi:10.1029/94JB02887.
Rychert, C. A., and P. M. Shearer (2009), A global view of the lithosphere-asthenosphere boundary, *Science*, *324*, 495–498, doi:10.1126/science.1169754.
Rychert, C. A., and P. M. Shearer (2011), Imaging the lithosphere-asthenosphere boundary beneath the Pacific using SS waveform modeling, *J. Geophys. Res.*, *116*, B07307, doi:10.1029/2010JB008070.
Rychert, C. A., K. M. Fischer, and S. Rondenay (2005), A sharp lithosphere–asthenosphere boundary imaged beneath eastern North America, *Nature*, *436*, 542–545, doi:10.1038/nature03904.
Rychert, C. A., S. Rondenay, and K. M. Fischer (2007), P-to-S and S-to-P imaging of a sharp lithosphere-asthenosphere boundary beneath eastern North America, *J. Geophys. Res.*, *112*, B08314, doi:10.1029/2006JB004619.
Rychert, C. A., P. M. Shearer, and K. M. Fischer (2010), Scattered wave imaging of the lithosphere–asthenosphere boundary, *Lithos*, *120*, 173–185, doi:10.1016/j.lithos.2009.12.006.
Rychert, C. A., N. Schmerr, and N. Harmon (2012), The Pacific lithosphere-asthenosphere boundary: Seismic imaging and anisotropic constraints from SS waveforms, *Geochem. Geophys. Geosyst.*, *13*, Q0AK10, doi:10.1029/2012GC004194.

Rychert, C. A., G. Laske, N. Harmon, and P. M. Shearer (2013), Seismic imaging of melt in a displaced Hawaiian plume, *Nat. Geosci.*, *6*, 657–660, doi:10.1038/ngeo1878.
Rychert, C. A., N. Harmon, and C. Ebinger (2014), Receiver function imaging of lithospheric structure and the onset of melting beneath the Galápagos Archipelago, *Earth Planet. Sci. Lett.*, *388*, 156–165, doi:10.1016/j.epsl.2013.11.027.
Sakamaki, T., A. Suzuki, E. Ohtani, H. Terasaki, S. Urakawa, Y. Katayama, K. I. Funakoshi, Y. Wang, J. W. Hernlund, and M. D. Ballmer (2013), Ponded melt at the boundary between the lithosphere and asthenosphere, *Nat. Geosci.*, *6*, 1041–1044. doi:10.1038/ngeo1982.
Schilling, J. (1991) Fluxes and excess temperatures of mantle plumes inferred from their interaction with migrating mid-ocean ridges, *Nature*, *352*, 397–403.
Schilling, J., R. Kingsley, and J. Devine (1982), Galápagos hot spot-spreading center system, 1. Spatial petrological and geochemical variations (83°W–101°W), *J. Geophys. Res.*, *87*, 5593–5610.
Schmerr, N. (2012), The Gutenberg discontinuity: Melt at the lithosphere-asthenosphere boundary, *Science*, *335*, 1480–1483, doi:10.1126/science.1215433.
Schutt, D. L., and C. E. Lesher (2006), Effects of melt depletion on the density and seismic velocity of garnet and spinel lherzolite, *J. Geophys. Res.*, *111*, B05401, doi:10.1029/2003JB002950.
Shen, Y., and D. W. Forsyth (1995), Geochemical constraints on initial and final depths of melting beneath mid-ocean ridges, *J. Geophys. Res.*, *100*, 2211–2237.
Shito, A., S. I. Karato, and J. Park, (2004), Frequency dependence of Q in Earth's upper mantle inferred from continuous spectra of body waves, *Geophys. Res. Lett.*, *31*, L12603, doi: 10.1029/2004GL019582.
Stixrude, L., and C. Lithgow-Bertelloni (2005), Mineralogy and elasticity of the oceanic upper mantle: Origin of the low-velocity zone, *J. Geophys. Res.*, *110*, B03204, doi:10.1029/2004JB002965.
Tan, Y., and D. V. Helmberger (2007), Trans-Pacific upper mantle shear velocity structure, *J. Geophys. Res.*, *112*, B08301, doi:10.1029/2006JB004853.
Tandon, G. P., and G. J. Weng (1984), The effect of aspect ratio of inclusions on the elastic properties of unidirectionally aligned composites, *Polym. Compos.*, *5*, 327–333, doi:10.1002/pc.750050413.
Till, C. B., T. L. Grove, R. W. Carlson, M. J. Fouch, J. M. Donnelly-Nolan, L. S. Wagner, and W. K. Hart (2013), Depths and temperatures of $<$10.5 Ma mantle melting and the lithosphere-asthenosphere boundary below southern Oregon and northern California, *Geochem. Geophys. Geosyst.*, *14*, 864–879, doi:10.1002/ggge.20070.
Tonegawa, T. and G. Helffrich (2012), Basal reflector under the Philippine Sea plate, *Geophys. J. Int.*, *189*, 659–668, doi:10.1111/j.1365-246X.2012.05386.x.
Turcotte, D. L., and G. Schubert (2002), *Geodynamics*, 2nd ed., 456 pp., Cambridge Univ. Press, New York.
Villagómez, D. R., D. R. Toomey, E. E. Hooft, and S. C. Solomon (2007), Upper mantle structure beneath the Galápagos Archipelago from surface wave tomography, *J. Geophys. Res.*, *112*, B07303, doi:10.1029/2006JB004672.
Villagómez, D. R, D. R. Toomey, E. E. Hooft, and S. C. Solomon (2011), Crustal structure beneath the Galápagos Archipelago from ambient noise tomography and its implications for plume-lithosphere interactions, *J. Geophys. Res.*, *116*, B04310, doi:10.1029/2010JB007764.
Villagómez, D., D. R. Toomey, D. J. Geist, E. E. E. Hooft, and S. C. Solomon (2014), Mantle flow and multistage melting beneath the Galápagos hotspot revealed by seismic imaging, *Nat. Geosci.*, *7*, 151–156, doi:10.1038/ngeo2062.
Vinnik, L. (1977), Detection of waves converted from P to SV in the mantle, *Phys. Earth Planet. Inter.*, *67*, 39–45, doi:10.1016/0031–9201(77)90008-5.
Vinnik, L. P., G. R. Foulger, and Z. Du (2005) Seismic boundaries in the mantle beneath Iceland: A new constraint on temperature, *Geophys. J. Int. 160*, 533–538, doi:10.1111/j.1365-246X.2005.02529.x.
Wagner, L. S., M. J. Fouch, D. E. James, and S. Hanson-Hedgecock (2012), Crust and upper mantle structure beneath the Pacific Northwest from joint inversion of ambient noise and earthquake data, *Geochem. Geophys. Geosyst.*, *13*, Q0AN03, doi:10.1029/2012GC004353.
Webb, S. C. (1998), Broadband seismology and noise under the ocean, *Rev. Geophys.*, *36*, 105–142, doi:10.1029/97RG02287.
White, W. M., A. R. McBirney, R. A. Duncan (1993), Petrology and geochemistry of the Galápagos Islands: Portrait of a pathological mantle plume, *J. Geophys. Res.*, *98*, 19,533–19,563, doi:10.1029/93JB02018.
Wölbern, I., A. W. B. Jacob, T. A. Blake, R. Kind, X. Li, X. Yuan, F. Duennebier, and M. Weber (2006), Deep origin of the Hawaiian tilted plume conduit derived from receiver functions, *Geophys. J. Int.*, *166*, 767–781, doi:10.1111/j.1365-246X.2006.03036.x.
Yang, Y., D. W. Forsyth, and D. S. Weeraratne (2007), Seismic attenuation near the East Pacific Rise and the origin of the low-velocity zone, *Earth Planet. Sci. Lett.*, *258*, 260–268, doi:10.1016/j.epsl.2007.03.040.